

Towards Large-scale Network Emulation on Analog Neuromorphic Hardware

Elias Arnold*
Philipp Spilger*
Jan V. Straub
Eric Müller

elias.arnold@kip.uni-heidelberg.de
Kirchhoff-Institute for Physics, Heidelberg University
Heidelberg, Germany

Gabriele Meoni
Faculty of Aerospace Engineering, Delft University of
Technology
Delft, The Netherlands

Dominik Dold
Advanced Concepts Team, European Space Research and
Technology Centre, European Space Agency
Noordwijk, The Netherlands

Johannes Schemmel
Kirchhoff-Institute for Physics, Heidelberg University
Heidelberg, Germany

ABSTRACT

We present a novel software feature for the BrainScaleS-2 accelerated neuromorphic platform that facilitates the emulation of partitioned large-scale spiking neural networks. This approach is well suited for many deep spiking neural networks, where the constraint of the largest recurrent subnetwork fitting on the substrate or the limited fan-in of neurons is often not a limitation in practice. We demonstrate the training of two deep spiking neural network models—using the MNIST and EuroSAT datasets—that exceed the physical size constraints of a single-chip BrainScaleS-2 system. The ability to emulate and train networks larger than the substrate provides a pathway for accurate performance evaluation in planned or scaled systems, ultimately advancing the development and understanding of large-scale models and neuromorphic computing architectures.

KEYWORDS

modeling, neuromorphic, spiking neural networks, space

1 INTRODUCTION

For traditional deep learning algorithms, whether simulated on conventional hardware or accelerated using graphics processing units (GPUs) and specialized hardware, the seamless integration of machine learning frameworks such as PyTorch and TensorFlow has simplified modeling and accelerated research. Recent years have seen a parallel evolution in the field of spiking neural networks (SNNs), where specialized modeling interfaces [10, 16] have begun to play a key role in streamlining the model development process. While the creation of a scaffold for building software support within machine learning libraries for general-purpose processing units is well established [4, 8], it is still an open research topic in the context of custom digital neuromorphic hardware [18], and even more so for the time-continuous nature of many analog neuromorphic systems, where the path to seamless integration is considerably more intricate.

In this work, we address typical model size limitations imposed by small substrates such as the BrainScaleS-2 (BSS-2) accelerated mixed-signal neuromorphic system, which is typically deployed in its single-chip variant. The BSS-2 architecture has been designed as a research vehicle for computational neuroscience, offering specialized features tailored to address the intricacies of neural dynamics and plasticity. The inclusion of multi-compartmental neurons, complex synapse dynamics, adaptive exponential integrate-and-fire (AdEx) compartment dynamics, as well as short-term and long-term plasticity, positions BSS-2 as a versatile platform for exploring diverse neural phenomena. Beyond computational neuroscience, BSS-2 also extends its reach into machine-learning-inspired applications, where functional modeling often draws inspiration from machine learning.

Typical deep neural networks (DNNs), and adapted models for spiking neurons, are often significantly larger than neuromorphic ASICs. While small-scale multi-chip system prototypes using an EXTOLL-based FPGA-mediated interconnect have been demonstrated in multiple use cases [23, 24], the majority of available BSS-2 system resources operate as single-chip configurations. However, networks with limited fan-in requirements that either comprise a pure feed-forward topology or sufficiently local recurrence allow for the partitioning into subnetworks that individually fit onto single ASICs. In general, partitioning introduces sequence points where emulation can be paused while the data flow still determines the execution order, i.e. subnetwork partitions of early layers are emulated before later layers, but the execution order within a layer is arbitrary. This allows us to reuse “computational units” (neurons and synapses) multiple times, similar to conventional von-Neumann architectures. This departs from traditional neuromorphic systems, which often allocate dedicated resources for each component of spiking neural networks. Recent work [13] laid out a partitioning method for mapping large-scale neural network models onto neuromorphic hardware. Along these lines, for hardware supporting non-time-continuous operation, Song et al. [19] describes a complete workflow from model specification to hardware execution. Previous work by the authors provided similar functionality for the

*Contributed equally.

non-spiking operation mode of BSS-2 [21] as well as for SNNs [20], both of which support hardware-in-the-loop (ITL) training.

The BSS-2 software stack aims to provide a user-friendly modeling application programming interface (API) that abstracts away from hardware-specific intricacies [11]. Over the course of its development, machine learning inspired training approaches have become increasingly popular. However, until recently, our modeling efforts were mostly limited to the size constraints of single BSS-2 ASICs. In this work, we focus on providing a framework for integrating such partitioning methods more generally, including for SNNs, into the BSS-2 software stack.

In the following, we focus on scenarios, such as feed-forward networks or those with sufficiently small recurrent subnetworks, where hardware reuse becomes a practical proposition. The overarching goal is to automate the process of making BSS-2 amenable to such cases, thereby extending its capabilities to emulate larger-than-substrate-sized networks efficiently and seamlessly. Finally, we demonstrate the training and emulation of larger, multi-partition networks on single-chip BSS-2 substrates using the MNIST [9] dataset of handwritten digits and the EuroSAT [6] dataset for land use and land cover classification. The latter is of particular relevance for future applications [7], as energy-efficient compute infrastructure such as neuromorphic hardware represents a promising candidate for neural solutions onboard spacecraft — especially miniaturized ones like CubeSats. Here, we present the first results on BSS-2 for such a benchmark.

2 METHODS

In this work, the latest BSS-2 ASIC [15] is used as a mixed-signal neuromorphic substrate. It features 512 (single-compartment) neurons implementing the AdEx model [1, 2] which can receive events via 256 synapses each. Events are propagated via digital signals, while the post-synaptic neuron dynamics evolve in the analog domain. Therefore, the emulation operates time-continuously and in real-time — in contrast to digital simulation, the experiment in general cannot be paused. Using the current default FPGA-ASIC link speed, the maximum sustained bandwidth is 250 MHz for both input and output.

Hence, the network size which can be concurrently (and inter-dependently) emulated is limited by the number of neuron and synapse circuits on the hardware. However, concurrent execution is only required for tightly-coupled recurrent network subgraphs, while feed-forward network subgraphs can be partitioned and run in parts. Figure 1 and fig. 2 sketch the partitioning of feed-forward (e.g., convolutions, receptive fields and dense) as well as recurrent projections.

Splitting networks into multiple partitions requires the events in between executions to be recorded and played back in dependent executions. This increases the required communication of events from and to the system compared to direct forwarding of events within the hardware. However, for typical machine-learning-inspired training the events from hidden layers are required in any case.

In general, partitioning projections does not necessarily decrease the fan-in for the post-synaptic layer. Thus, we take advantage of the hardware’s ability to combine neuron circuits, resulting in an

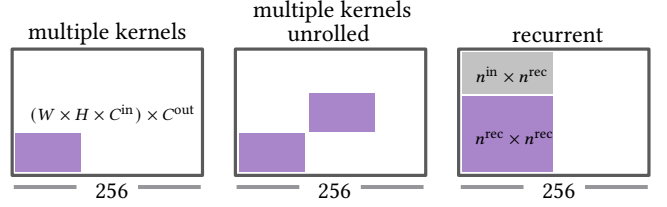


Figure 1: Partitioning of convolutional and recurrent projections. (left) Parallel execution of C^{out} (horizontal) kernels at one input position per run. (middle) Parallel execution of C^{out} (horizontal) kernels at multiple (vertical) input positions per run. (right) Recurrently connected layers must be placed simultaneously on the neuromorphic substrate. The recurrent projection reduces the size of the remaining fan-in.

increased fan-in capability of ‘ $256 \cdot \text{\#neuron circuits per neuron}$ ’, up to $256 \times 64 = 16384$ unsigned weights. We use two 6 bit-weight hardware synapses to represent a signed weight, therefore the maximum number of signed input weights is 8192. Consequently, this decreases the number of ‘logical’ neurons available per single execution by $\text{\#neurons} = \frac{512}{\text{\#neuron circuits per neuron}}$, possibly leading to more partitions.

The BSS-2 software stack follows a layered approach: starting with a transport layer, the configuration abstraction is implemented using a container-coordinate scheme for type safety and user-readable configuration [12]. The natural experiment notation for highly event-driven neuromorphic hardware is a signal-flow-graph-based notation [11], which serves as a backend for the neuroscience and machine-learning frontends. It represents both the on-chip signal flow — events and analog signals — and the off-chip data flow. To take advantage of developments in the machine learning community, the user-facing API [20] is based on PyTorch data structures and integrates with its auto-differentiation functionality.

2.1 Training

The MNIST and EuroSAT models are trained using well-established surrogate gradient-based learning methods [14]. Class scores are optimized by minimizing the cross-entropy loss, using the Adam optimizer with (surrogate) gradients obtained by the backpropagation through time (BPTT) algorithm. To approximate the networks’ gradients on BSS-2, we apply the hardware-in-the-loop (ITL) training procedure [17] and read out the network observables, i.e. membrane voltages and spikes. These observables are mapped to a PyTorch tensor with a fixed time grid with resolution δt . For this, we calculate the factor which scales the membrane dynamics on BSS-2 to the corresponding dynamics in software, that are expected for gradient estimation. Synapse and neuron dynamics are numerically integrated on this time lattice in the case of simulated (sub-)networks. Each part of the network is run, or simulated respectively, for $30 \mu\text{s}$ in the case of MNIST and $64 \mu\text{s}^1$ in the case of EuroSAT per image.

¹Plus an added safety margin in BSS-2 to ensure a desired amount of membrane measurements.

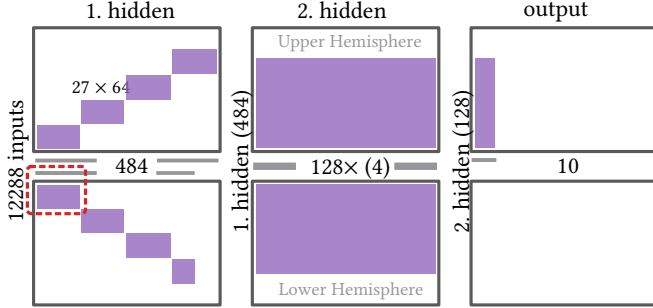


Figure 2: Partitioning and placement of the network used to classify the EuroSAT dataset. The basic synapse and neuron layout of the BSS-2 ASIC is shown in each column: in the center, two rows of neuron circuits are located; each neuron row is fed from the adjacent synapse array (top/bottom rectangles). Neuron circuits can be combined to form larger logical neurons, supporting larger fan in. On the left of each hardware instance, the source and size of the fan-in are indicated. Each neuron in the first hidden layer has a receptive field of $3 \times 3 \times 3$ and can be mapped to one BSS-2 instance. To reduce the number of input spikes, we run it in multiple parts (indicated by the red box). The neurons in the second layer consist of four connected neuron circuits. This layer, as well as the readout layer, is executed in a single run each.

2.2 MNIST Dataset & Model

The MNIST dataset contains 70 000 28×28 gray scale images of handwritten digits that are categorized into 10 classes (0 to 9). 60 000 images are meant for training purposes, the rest for testing the model. In our case the images are cropped to a size of 22×22 and we consider a fully connected feed-forward network with 256 leaky-integrate and fire (LIF) features in the hidden layer and 10 leaky integrators (LIs) in the readout layer. A time-to-first spike (TTFS) encoding scheme that is specified in section 3.2.1 transfers the images from a pixel-value representation to spike events. The measured/simulated membrane traces v_k at the readout layer are converted into scores s_k for the different classes by a max-over-time decoding, $s_k = \max_t (v_k(t))$ [3]. The dataset is augmented by using random rotations up to 25° which are applied with a probability of 50% and differ for each epoch of the training process. As the images lose a bit of brightness when rotating with the bilinear interpolation method, they are brightened up by a factor of 1.5 and clipped at the maximum value of 1.0. For improved generalization we also use dropout with a probability of 15% in the hidden layer, resulting in some of the hidden spikes not being injected into the readout layer during training. For testing, dropout is disabled.

2.2.1 Regularization on BSS-2. To keep the network’s dynamics and parameters within the system capabilities, we use regularization terms that extend the loss function. Of particular interest are the firing rate in the hidden layer which might exceed the system’s bandwidth, the read out membrane traces which might saturate due to the limited range of the columnar ADC (ADC) and the weights which are also limited in range on hardware.

2.2.2 Training. The training process spans 100 epochs during which the learning rate and firing rate regularization constant decrease exponentially. At the end of each training, the model’s performance is evaluated with the test set. The final performance of our setup is the average over specific model performances using the same parameters but different pseudorandom number generator (PRNG) seeds.

2.3 EuroSAT Dataset & Model

The EuroSAT dataset consists of 27 000 $64 \times 64 \times 3$ RGB² images of the Earth’s surface taken by the satellite mission Sentinel-2, categorized into 10 classes. We split the dataset in training, validation, and test set by ratios 0.7, 0.1, and 0.2. For regularization, random flips are applied to the training images. For its classification, we consider a network with two hidden LIF layers and one LI readout layer to infer decisions. For spike encoding of the input images we use a TTFS and a multiple-spike encoding scheme. While the first allows only one spike per neuron in the input layer, the latter has no such restriction, see section 3.3.1. Class scores s_k are obtained by taking the membrane value $v_k(t = T)$ of the LI neurons at the end of the considered time frame T .

2.3.1 Training. In addition to the training procedure outlined in section 2.1, we halve the learning rate after the epochs 10, 20, 30, 40, 50 and 60. Training is performed for a maximum of 500 epochs in simulation, or 100 on BSS-2. If there is no improvements on the validation accuracy for 25 epochs in simulation or 15 epochs on BSS-2, the training is stopped. We save the best performing model on the validation set and use it for later evaluation on the test set. A summary of all model and training parameters is given in table 1.

3 RESULTS

In this section we describe our software support for model partitioning and sequential execution on BSS-2, exemplified on the MNIST and EuroSAT datasets.

3.1 Software

While a user of a machine learning framework does not need to know the partitioning, this information is required in the intermediate representation used for scheduling execution on hardware. There, networks are comprised of populations of neurons and projections of synapses. In the experiment notation backend, the ability of the signal-flow graph to represent multiple executions and their data-flow dependencies can be used to represent partitioned networks. For this, we annotate network entities with information about to which execution they belong to. Event forwarding from one execution to another is represented by an inter-execution projection (without using hardware synapses) receiving recorded events from the source execution and injecting these events to the target execution. We use the host computer for translation of the events, which allows complete decoupling of event routing constraints between executions.

In the machine learning frontend `hxtorch.snn`, each layer is assigned to a specific execution via a parameter upon construction. The inter-execution dependencies are then automatically extracted

²We only consider the RGB bands out of the 13 provided spectral bands.

from the call graph. This enables explicit (manual) partitioning as well as employing user-defined partitioning algorithms, which can also be used for mixed hardware and simulation networks, see section 3.3. Figure 5 shows the frontend API in use exemplarily for the network used for MNIST classification, the corresponding data flow is visualized in fig. 4.

Due to multiple partially sequential executions and increased required data transfer when using multiple partitions in contrast to executing a network in a single hardware run, runtime performance impairment is expected. The hardware runtime scales linearly with the depth of the partitioned network, since these executions are required to be run sequentially due to inter-partition data dependencies. Partitions without data dependencies, e.g., multiple partitions of the same layer, can be executed concurrently depending on the available hardware resources. Therefore, runtime additionally scales linearly with the ratio of concurrently executable partitions to available hardware. When partitioning all events between partitions are recorded and translated on the host computer. In contrast, networks executed in a single non-partitioned hardware run only require complete event recording during training, as only the data from the last layer is typically of interest during inference. In addition, event recording and translation overhead is expected to impair runtime performance in comparison to non-partitioned experiments. A dedicated inter-execution memory buffer in field-programmable gate array (FPGA)-managed dynamic random-access memory (DRAM) could at least eliminate the software overhead at the cost of additional FPGA development effort to support additional translation and playback of recorded data.

3.2 MNIST

Executing the network described in section 2.2 with the BSS-2 system is only possible after partitioning it into three parts as the 22×22 inputs require multiple neuron circuits to be connected. In particular, the 484 pixels are mapped to the same number of signed weights per neuron, requiring two hardware synapses each, thereby requiring four combined neuron circuits. By halving the hidden layer, the remaining 128 units comply with the BSS-2 restrictions ($128 \times 4 = 512$, the number of neuron circuits on the chip) so that each of the halves can be executed in one run. Once the spike events have been read out from the two halves of the hidden layer they can be reassembled in software—or by the FPGA—which is required to execute the readout layer. Figure 3 showcases a schematic view of the network and the necessary partitions for execution on BSS-2 and fig. 5 provides a software example of an explicitly partitioned network in `hxtorch.snn`. Section 3.2.1 details the used pixel-to-spike encoding.

3.2.1 Input Encoding. The particular TTFS encoding used here assigns spike times t_i^s to pixel values x_i in a linear manner,

$$x_i \rightarrow T \cdot \frac{x_i - x_{\min}}{x_{\max} - x_{\min}} =: f(x_i), \quad (1)$$

$$t_i^s = (T - \lfloor f(x_i) \rfloor) \cdot \delta t, \quad (2)$$

where T is the sequence length per image (set to $T = 30$), that together with the time interval $\delta t \equiv 1 \mu\text{s}$ determines the encoding resolution. The mixed flooring and ceiling brackets indicate

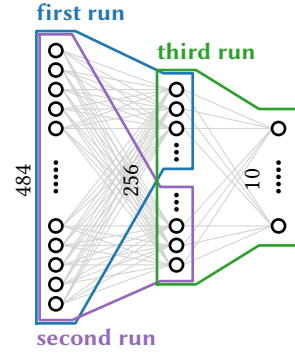


Figure 3: Schematic network topology for a network of $22 \times 22 \rightarrow 256 \rightarrow 10$ neurons. Partitions that can be run consecutively on hardware are marked. The two partitions in the first layer are interchangeable.

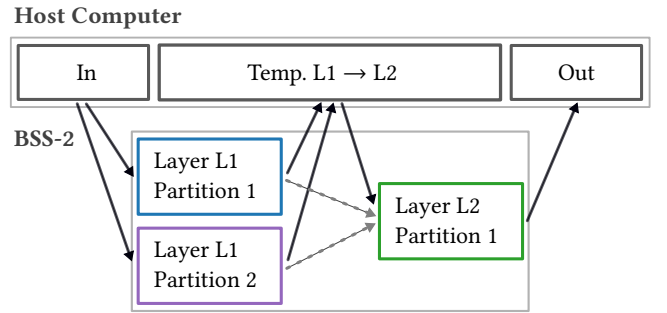


Figure 4: Data flow of the model from fig. 3 using three partitions, where the additional need to record and playback events to/from the host computer in-between layers is visualized.

rounding to the next integer (towards zero) and $x_{\min/\max}$ are the minimum (maximum) values 0 and 1 of the MNIST data set.

3.2.2 Training. Previously published models classifying MNIST [9] on BSS-2 used a scaled-down image size of 16×16 to reduce input dimensionality, reaching a test accuracy of $96.9 \pm 0.1\%$ [5] and $97.6 \pm 0.1\%$ [3] with dropout and augmentation. Our model with larger input dimension of 22×22 and a slightly larger hidden layer (256 compared to 246 before; see fig. 3) reaches $98.0 \pm 0.1\%$ using similar training methods. While the slightly improved MNIST classification performance alone does not emphasize the need for means to run larger scale models, it is an important milestone to validate our implementation and hardware operation against previous results.

3.3 EuroSAT

We trained the model described in section 2.3 to classify the EuroSAT dataset. Its partitioning and placement on BSS-2 is visualized in fig. 2.

Instead of densely projecting the large input space onto the first hidden layer, each neuron in the layer has a small receptive field of $3 \times 3 \times 3$ pixels. The receptive fields are moved over the spatial


```

first = hxtorch.snn.ExecutionInstanceID(1)
second = hxtorch.snn.ExecutionInstanceID(2)
third = hxtorch.snn.ExecutionInstanceID(3)

exp = hxtorch.snn.Experiment()

syn1 = hxtorch.snn.Synapse(exp, first, ...)
lif1 = hxtorch.snn.LIF(exp, first, ...)
syn2 = hxtorch.snn.Synapse(exp, second, ...)
lif2 = hxtorch.snn.LIF(exp, second, ...)
syn3 = hxtorch.snn.Synapse(exp, third, ...)
syn4 = hxtorch.snn.Synapse(exp, third, ...)
li3 = hxtorch.snn.LI(exp, third, ...)

x1 = syn1(input)
x2 = syn2(input)
x3 = lif1(x1)
x4 = lif2(x2)
x5 = syn3(x3)
x6 = syn4(x4)
x7 = li3(x5)
x7 = li3(x6)

hxtorch.snn.run(exp, ...)

loss = f(x7)
loss.backward()

```

Figure 5: Software API of explicitly partitioned network in hxtorch.snn shown exemplarily for the MNIST network.

coordinates (height and width) of the image with stride 3, resulting in each neuron receiving a unique set of input pixels. For the BSS-2 system this encoding is particularly convenient since it makes use of the system’s intrinsic support for placing sparse connections. With the given size of the receptive field, the first hidden layer has a size of 484 neurons with 27 inputs each. Each synapse row on BSS-2 can distinguish 64 event labels, hence, we uniquely address a maximum of 64 neurons through the same row. This allows to map the sparse projection in blocks of 27×64 “signed” hardware synapses onto BSS-2 and thus run the whole first layer at once. Given the large number of spike events, due to the size of the input space, means for reducing the number of input events are applied – also by partitioning of the first hidden layer, thereby reducing the number of input neurons required per execution (see red box in fig. 2). In case of TTFS input encoding, we execute this layer in 8 parts, resulting in 10 executions needed to emulate the whole network. For the multi-spike encoding, we divide this layer into 4 parts, yielding 6 partitions in total. The remaining projections between layers have all-to-all connectivity. We choose a second hidden layer of size 128, which can be emulated within one run by connecting four neuron circuits on BSS-2 to form one neuron in order to support a fan-in of 484 from the previous layer. The readout layer is implemented with single-circuit neurons.

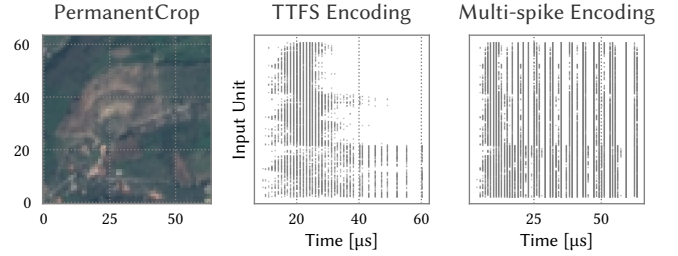


Figure 6: (left) Example image of the EuroSAT dataset. (middle) The image TTFS encoded. (right) The image multi-spike encoded.

3.3.1 Input Encoding. We investigate two different spike encodings of the input images. First, we look at a single-event TTFS and, second, at a multi-spike encoding scheme. Parameters are given in table 1.

Single-spike. To avoid the on-chip spike event rate to exceed the system’s bandwidth, we use an TTFS input encoding scheme, see fig. 6. Each pixel value $x_i \in [0, 1]$ is interpreted as a constant current onto a LIF neuron with an infinite refractory period, i.e. the neuron can only spike once at t_i^s (cf. [3]). This yields an early spike time for stronger pixel intensities and silent neurons if the pixel value is too small. We add a bias value x_{\min} to x_i to bias the inputs towards early spiking. The spike times t_i^s are numerically computed according to

$$\dot{v}_i(t) = -\frac{1}{\tau_{\text{en}}}v_i(t) + x_i + x_{\min} \longrightarrow t_i^s = t|_{v_i(t)=\vartheta_{\text{en}}}, \quad (3)$$

with v_i being a membrane state, and ϑ_{en} the threshold. See fig. 6 (middle) for an example. Using this encoding, we achieve an average spike count per time bin of 162 (averaged over training set and time bins) and the maximum average spike count encountered in a bin (averaged over training set) to 527.

The BSS-2 FPGA only processes two spikes per clock cycle, i.e. simultaneous sends might get delayed. If the maximum bandwidth is exceeded for longer time spans, spikes are dropped. To minimize simultaneous events, we compute the spike times at FPGA resolution. However, since the dataset is constituted of only 252 unique pixel values only the same number of unique spike times will occur. In the forward direction, we therefore jitter the pixel images by adding Gaussian noise, $x_i + \mathcal{N}(\mu = 0, \sigma_{\text{in}})$. For gradient optimization we assume the same resolution δt as in the simulations.

Multi-spike. Here, each pixel x_i is interpreted as a constant current onto a LIF neuron which emits the set of spike events $\{t_{i,k}^s\}$. While small pixel intensities might yield silent neurons, larger values result in multiple spikes over time. An example is shown in fig. 6 (right).

We observe approximately 1062 spikes in each time step (averaged over training set and bins), with an average maximum spike count of 3906 in a single time bin (averaged over training set). Hence, the spike counts per time step exceed the supported input rate on BSS-2 per μs by one order of magnitude. This will lead to spike drops and/or delayed spike events on chip.

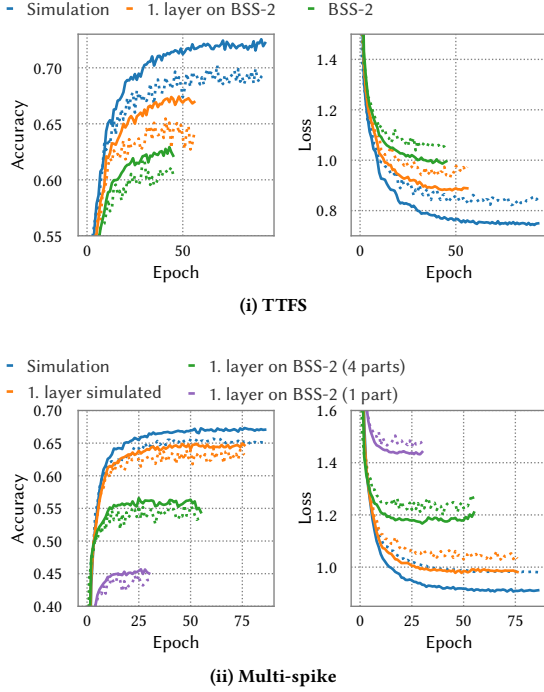


Figure 7: Accuracy (left) and loss (right) of the model on the EuroSAT dataset in simulation and/or in BSS-2. The solid lines correspond to the training set, the dotted to the validation set. (i) TTFS network performance in simulation (blue), and on BSS-2: only first layer (orange), full network (green). (ii) Multi-spike network performance in simulation (blue), and on BSS-2: first hidden layer in software and the remaining model on BSS-2 (orange), first hidden layer on BSS-2 split into four partitions (green), first hidden layer on BSS-2 without any partitioning (violet),

3.3.2 Training. In fig. 7i we show the training (solid) and validation (dotted) accuracy and loss of our model on the EuroSAT dataset [6]. Using the TTFS input encoding, we achieve a test accuracy of 69.5% (blue) in a software-only training. When emulating the whole model on BSS-2 (green) the test accuracy is 61.9%. We showcase an example of mixed software / BSS-2 execution where only the first hidden layer is run on BSS-2 (orange).

Figure 7ii depicts the training and validation accuracy when using the multi-spike encoding. With a simulated baseline model, we achieve 65.4% test accuracy (blue). We observe a small hardware penalty, when we only run the first hidden layer in software and the remaining model on BSS-2 (orange). Vice versa, if the first hidden layer is run on BSS-2 without any partitioning, the training and validation accuracy decrease significantly (violet). In comparison, partitioning said layer into four parts and run it sequentially increases the performance (green).

4 DISCUSSION

This paper highlights the significance of novel software support facilitating the emulation of partitioned large-scale SNNs on the BSS-2 neuromorphic substrate. Manual partitioning of suitable SNN topologies is always an option, but the integration of software support into the BSS-2 software stack helps researchers to shift their focus from system handling to modeling.

We demonstrated the software feature on models classifying the MNIST and EuroSAT datasets. To validate our implementation, we used the MNIST dataset as there are several publications using single-chip BSS-2 systems, we perform slightly better on 22×22 image resolution than the smaller models on 16×16 images, achieving $98.0 \pm 0.1\%$ test accuracy, see section 3.2 for details. This is the best performance on MNIST recorded on BSS-2 so far. We acknowledge that superior input encoding and training setup may also contribute to this improvement.

For the larger EuroSAT task, we present the first results obtained on BSS-2. We showcase the emulation of the largest SNN to date on BSS-2 by means of partitioning into subnetworks, each of which is executable on a single substrate. Thanks to the sparse input projection we were able to map a 12288-dimensional input space to hardware. Due to connectivity sparsity, the first hidden layer is emulated in 8 parts, resulting in 10 partitions for the whole network. In the future, sufficiently large multi-chip systems will be able to emulate all partitions concurrently. While focusing on the mapping of the model to BSS-2, the sequential execution of the model resulted in a test accuracy of 61.9%, thus supporting our presented approach for large-scale model emulation. The performance gap to the simulation is assumed to be not inherent to the analog nature of the system. Reasons for performance degradation on BSS-2 can be suboptimal hardware operation points and training setup, in addition to spike loss in the input layer due to bandwidth constraints. We are optimistic to resolve the latter by stretching the experiment temporally in order to minimize the number of simultaneous events and by increasing the number of partitions of the first hidden layer. The latter is suggested by the multi-spike experiments where an increasing number of partitions result in better validation accuracy.

While partitioned emulation is typically superlinearly slower than on a sufficiently large substrate, the ability to explore larger networks is valuable, especially when considering typical hardware development cycle times and costs. Due to the mixed-signal nature of the BSS-2 architecture—and many other neuromorphic systems [22]—the partitioning of SNNs does not affect the emulation fidelity compared to a system with network-matching system size: spikes are events in time that can be reliably recorded (within the constraints of the system’s I/O bandwidth) and played back at later points in time, thereby providing deterministic communication between subnetworks. The ability to facilitate answering questions about the desired model and hardware system size with the confidence of a realistic emulation is a key outcome of this work. This not only addresses the immediate need to understand the behavior of larger networks on existing hardware, but also provides valuable insight into the feasibility and performance expectations for future, more expansive—and expensive—neuromorphic systems.

ACKNOWLEDGMENTS

The authors wish to thank all present and former members of the Electronic Vision(s) research group contributing to the BrainScaleS-2 neuromorphic platform.

This work has received funding from the EC Horizon 2020 Framework Programme under grant agreements 785907 (HBP SGA2) and 945539 (HBP SGA3), the EC Horizon Europe Framework Programme under grant agreement 101147319 (EBRAINS 2.0), the Deutsche Forschungsgemeinschaft (DFG, German Research Foundation) under Germany’s Excellence Strategy EXC 2181/1-390900948 (the Heidelberg STRUCTURES Excellence Cluster), the German Federal Ministry of Education and Research under grant number 16ES1127 as part of the *Pilotinnovationswettbewerb ‘Energieeffizientes KI-System’*, the Helmholtz Association Initiative and Networking Fund [Advanced Computing Architectures (ACA)] under Project SO-092, and the Lautenschläger-Forschungspreis 2018 for Karlheinz Meier. This study has been supported by the European Space Agency’s Ariadna scheme (Study Ref. 4000136024/21/NL/GLC/my).

AUTHOR CONTRIBUTIONS

EA & JVS: Investigation, visualization, methodology, software, writing – original draft, writing – reviewing & editing; EA: Conceptualization; PS & EM: Conceptualization, methodology, software, writing – original draft, writing – reviewing & editing; EM: Supervision; DD & GM: Methodology, resources, validation, writing – original draft & editing. JS: Methodology, supervision, resources, funding acquisition, writing – reviewing & editing.

REFERENCES

- [1] Sebastian Billaudelle, Johannes Weis, Philipp Dauer, and Johannes Schemmel. 2022. An accurate and flexible analog emulation of AdEx neuron dynamics in silicon. In *2022 29th IEEE International Conference on Electronics, Circuits and Systems (ICECS)*. 1–4. <https://doi.org/10.1109/ICECS202256217.2022.9971058>
- [2] R. Brette and W. Gerstner. 2005. Adaptive Exponential Integrate-and-Fire Model as an Effective Description of Neuronal Activity. *J. Neurophysiol.* 94 (2005), 3637–3642. <https://doi.org/10.1152/jn.00686.2005>
- [3] Benjamin Cramer, Sebastian Billaudelle, Simeon Kanya, Aron Leibfried, Andreas Grübl, Vitali Karasenko, Christian Pehle, Korbinian Schreiber, Yannik Stradmann, Johannes Weis, et al. 2022. Surrogate gradients for analog neuromorphic computing. *Proceedings of the National Academy of Sciences* 119, 4 (2022). <https://doi.org/10.1073/pnas.2109194119>
- [4] Facebook, Inc. 2021. *PyTorch on XLA Devices*. <https://pytorch.org/xla/release/1.9/index.html>
- [5] Julian Göltz, Laura Kriener, Andreas Baumbach, Sebastian Billaudelle, Oliver Breitwieser, Benjamin Cramer, Dominik Dold, Ákos Ferenc Kungl, Walter Senn, Johannes Schemmel, Karlheinz Meier, and Mihai A. Petrovici. 2021. Fast and energy-efficient neuromorphic deep learning with first-spike times. *Nature Machine Intelligence* 3, 9 (2021), 823–835. <https://doi.org/10.1038/s42256-021-00388-x>
- [6] Patrick Helber, Benjamin Bischke, Andreas Dengel, and Damian Borth. 2017. EuroSAT: A Novel Dataset and Deep Learning Benchmark for Land Use and Land Cover Classification. (Aug. 2017). <https://doi.org/10.1109/JSTARS.2019.2918242>
- [7] Dario Izzo, Alexander Hadjiivanov, Dominik Dold, Gabriele Meoni, and Emmanuel Blazquez. 2022. Neuromorphic Computing and Sensing in Space. In *Artificial Intelligence for Space: AI4SPACE*. CRC Press, 107–159.
- [8] Chris Lattner, Mehdi Amini, Uday Bondhugula, Albert Cohen, Andy Davis, Jacques Pienaar, River Riddle, Tatiana Shpeisman, Nicolas Vasilache, and Oleksandr Zinenko. 2021. MLIR: Scaling Compiler Infrastructure for Domain Specific Computation. In *2021 IEEE/ACM International Symposium on Code Generation and Optimization (CGO)*. 2–14. <https://doi.org/10.1109/CGO51591.2021.9370308>
- [9] Yann LeCun and Corinna Cortes. 1998. The MNIST database of handwritten digits.
- [10] Davide L. Manna, Alex Vicente-Sola, Paul Kirkland, Trevor J. Bihl, and Gaetano Di Caterina. 2023. Frameworks for SNNs: A Review of Data Science-Oriented Software and an Expansion of SpykeTorch. In *Engineering Applications of Neural*

Table 1: EuroSAT Experiment Parameters

Batch size	64
Learning rate	0.001
Max. epochs (Sim./BSS-2)	25 / 15
Learning rate decay	0.5 in epochs 10, . . . , 60
Vertical/Horizontal flip	With 50 % probability
Optimizer	Adam with default params.
δt	1 μ s
Time steps T	64
Leakage potential	0
Reset potential	0
TTFS Experiments	
Encoder threshold ϑ_{en}	0.32
Encoder time constant τ_{en}	20 μ s
x_{min}	0.1
σ_{in}	0.003
Syn. time const.	[10, 10, 10] μ s
Mem. time const.	[10, 10, 10] μ s
Thresholds ϑ	[1, 1, –]
SuperSpike slope α	[10, 10, –]
Multi-spike Experiments	
Encoder threshold ϑ_{en}	0.1
Encoder time constant τ_{en}	33.3 μ s
Syn. time const. (Sim./BSS-2)	[100/30, 20, 13.3] μ s
Mem. time const. (Sim./BSS-2)	[100/60, 20, 13.3] μ s
Thresholds ϑ	[3, 2, –]
SuperSpike slope α	[1, 1, –]

- Networks*, Lazaros Iliadis, Ilias Maglogiannis, Serafin Alonso, Chrisina Jayne, and Elias Pimenidis (Eds.). Springer Nature Switzerland, Cham, 227–238.
- [11] Eric Müller, Elias Arnold, Oliver Breitwieser, Milena Czierlinski, Arne Emmel, Jakob Kaiser, Christian Mauch, Sebastian Schmitt, Philipp Spilger, Raphael Stock, Yannik Stradmann, Johannes Weis, Andreas Baumbach, Sebastian Billaudelle, Benjamin Cramer, Falk Ebert, Julian Göltz, Joscha Ilmberger, Vitali Karasenko, Mitja Kleider, Aron Leibfried, Christian Pehle, and Johannes Schemmel. 2022. A Scalable Approach to Modeling on Accelerated Neuromorphic Hardware. *Front. Neurosci.* 16 (2022). <https://doi.org/10.3389/fnins.2022.884128>
- [12] Eric Müller, Christian Mauch, Philipp Spilger, Oliver Julien Breitwieser, Johann Klähn, David Stöckel, Timo Wunderlich, and Johannes Schemmel. 2020. *Extending BrainScaleS OS for BrainScaleS-2*. Technical Report. Electronic Vision(s), Kirchhoff Institute for Physics, Heidelberg University, Germany, Heidelberg, Germany. <https://doi.org/10.48550/arXiv.2003.13750> arXiv:2003.13750 [cs.NE]
- [13] Nishant Mysore, Gopabandhu Hota, Stephen R. Deiss, Bruno U. Pedroni, and Gert Cauwenberghs. 2022. Hierarchical Network Connectivity and Partitioning for Reconfigurable Large-Scale Neuromorphic Systems. *Frontiers in Neuroscience* 15 (2022). <https://doi.org/10.3389/fnins.2021.797654>
- [14] Emre O. Neftci, Hesham Mostafa, and Friedemann Zenke. 2019. Surrogate gradient learning in spiking neural networks: Bringing the power of gradient-based optimization to spiking neural networks. *IEEE Signal Processing Magazine* 36, 6 (2019), 51–63. <https://doi.org/10.1109/MSP.2019.2931595>
- [15] Christian Pehle, Sebastian Billaudelle, Benjamin Cramer, Jakob Kaiser, Korbinian Schreiber, Yannik Stradmann, Johannes Weis, Aron Leibfried, Eric Müller, and Johannes Schemmel. 2022. The BrainScaleS-2 Accelerated Neuromorphic System with Hybrid Plasticity. *Frontiers in Neuroscience* 16 (2022). <https://doi.org/10.3389/fnins.2022.795876>
- [16] Christian Pehle and Jens Egholm Pedersen. 2021. *Norse – A deep learning library for spiking neural networks*. <https://doi.org/10.5281/zenodo.4422025> Documentation: <https://norse.ai/docs/>.
- [17] Sebastian Schmitt, Johann Klähn, Guillaume Bellec, Andreas Grübl, Maurice Güttler, Andreas Hartel, Stephan Hartmann, Dan Husmann, Kai Husmann, Sebastian Jeltsch, Vitali Karasenko, Mitja Kleider, Christoph Koke, Alexander Kononov, Christian Mauch, Eric Müller, Paul Müller, Johannes Partzsch, Mihai A. Petrovici, Bernhard Vogginger, Stefan Schiefer, Stefan Scholze, Vasilis

- Thanasoulis, Johannes Schemmel, Robert Legenstein, Wolfgang Maass, Christian Mayr, and Karlheinz Meier. 2017. Neuromorphic Hardware In The Loop: Training a Deep Spiking Network on the BrainScaleS Wafer-Scale System. *Proceedings of the 2017 IEEE International Joint Conference on Neural Networks (2017)*. <https://doi.org/10.1109/IJCNN.2017.7966125>
- [18] Amar Shrestha, Haowen Fang, Zaidao Mei, Daniel Patrick Rider, Qing Wu, and Qinru Qiu. 2022. A Survey on Neuromorphic Computing: Models and Hardware. *IEEE Circuits and Systems Magazine* 22, 2 (2022), 6–35. <https://doi.org/10.1109/MCAS.2022.3166331>
- [19] Shihao Song, Adarsha Balaji, Anup Das, Nagarajan Kandasamy, and James Shackelford. 2020. Compiling Spiking Neural Networks to Neuromorphic Hardware. In *The 21st ACM SIGPLAN/SIGBED Conference on Languages, Compilers, and Tools for Embedded Systems (London, United Kingdom) (LCTES '20)*. Association for Computing Machinery, New York, NY, USA, 38–50. <https://doi.org/10.1145/3372799.3394364>
- [20] Philipp Spilger, Elias Arnold, Luca Blessing, Christian Mauch, Christian Pehle, Eric Müller, and Johannes Schemmel. 2023. hxtorch.snn: Machine-learning-inspired Spiking Neural Network Modeling on BrainScaleS-2. In *Neuro-inspired Computational Elements Workshop (NICE 2023)* (University of Texas, San Antonio, USA). Association for Computing Machinery, New York, NY, USA, 57–62. <https://doi.org/10.1145/3584954.3584993> arXiv:2212.12210 [cs.NE]
- [21] Philipp Spilger, Eric Müller, Arne Emmel, Aron Leibfried, Christian Mauch, Christian Pehle, Johannes Weis, Oliver Breitwieser, Sebastian Billaudelle, Sebastian Schmitt, Timo C. Wunderlich, Yannik Stradmann, and Johannes Schemmel. 2020. hxtorch: PyTorch for BrainScaleS-2 — Perceptrons on Analog Neuromorphic Hardware. In *IoT Streams for Data-Driven Predictive Maintenance and IoT, Edge, and Mobile for Embedded Machine Learning*. Springer International Publishing, Cham, 189–200. https://doi.org/10.1007/978-3-030-66770-2_14
- [22] Chetan Singh Thakur, Jamal Lottier Molin, Gert Cauwenberghs, Giacomo Indiveri, Kundan Kumar, Ning Qiao, Johannes Schemmel, Runchun Wang, Elisabetta Chicca, Jennifer Olson Hasler, Jae-sun Seo, Shimeng Yu, Yu Cao, André van Schaik, and Ralph Etienne-Cummings. 2018. Large-Scale Neuromorphic Spiking Array Processors: A Quest to Mimic the Brain. *Front. Neurosci.* 12 (2018), 891. <https://doi.org/10.3389/fnins.2018.00891>
- [23] Tobias Thommes. 2023. *Interconnect Technologies for Very Large Spiking Neural Networks*. Ph. D. Dissertation. Ruprecht-Karls-Universität Heidelberg. <https://doi.org/10.11588/heidok.00034189>
- [24] Tobias Thommes, Sven Bordukat, Andreas Grübl, Vitali Karasenko, Eric Müller, and Johannes Schemmel. 2022. Demonstrating BrainScaleS-2 Inter-Chip Pulse Communication using EXTOLL. In *Neuro-inspired Computational Elements Workshop (NICE '22), March 29 – April 1, 2022* (Virtual Event, USA). Association for Computing Machinery, New York, NY, USA, 98–100. <https://doi.org/10.1145/3517343.3517376> arXiv:2202.12122 [cs.AR]